AAS 13-824

APPLICATION OF OPTICAL TRACKING AND ORBIT ESTIMATION TO SATELLITE ORBIT TOMOGRAPHY

Michael A. Shoemaker[*], Brendt Wohlberg[†], Richard Linares[‡], and Josef Koller[§]

Satellite orbit tomography is shown through numerical simulations to reconstruct the spatially-resolved global neutral density field using only a single ground site. The study assumes a ground site located near Los Alamos, New Mexico, and selects nearly 200 resident space objects in low-Earth orbit as potential tracking targets. Over a chosen six-day time span in 2011, around 50 objects have enough visibilities to be used. A Constrained Admissible Region Multiple Hypothesis Filter (CAR-MHF) is tested for estimating the satellite position, velocity, and drag ballistic coefficients. The CAR-MHF has difficulty estimating the state in these simulations when the assumed density model has large discrepancies compared with the truth model; however, the simulation results provide reasonable estimates of the expected orbit estimation accuracy for the chosen system. Using this information, the tomography is simulated for the remaining objects, and the density field at lower altitudes around 412 km is reconstructed to within several precent of the true time-averaged density values.

INTRODUCTION

A new method, inspired by computed tomography (CT) used in medical imaging, was recently developed for atmospheric density estimation using satellite orbits.[1,2] To summarize the method: the measured satellite orbital decay (i.e. change in specific mechanical energy) is used as the measurement, in place of the X-ray intensity loss used in CT scanners. The global density field is partitioned into a grid, and the density scale factor (i.e. a scalar correction to the modeled density) is solved for in each grid element. In past simulations, the method was used with 100 satellites and a grid with around 300 elements spanning an altitude range from 300 to 500 km altitude. This ill-posed problem was solved using Tikhonov regularization, with the 3D gradient chosen as the regularization operator, resulting in a penalty on the spatial smoothness of the estimated density. Preliminary simulations showed that the true time-averaged density could be reconstructed to within approximately 10%, using only simulated orbit estimates separated over 5 orbital revolutions.

The previous simulations used several simplifying assumptions for the purposes of that preliminary feasibility study: (1) the set of target satellites was randomly generated, such that there was sufficient orbital variety, (2) ground sites for orbit estimation were not specified, and instead it was

[*]Postdoctoral Research Associate, Space Science and Applications (ISR-1), Los Alamos National Laboratory, P.O. Box 1663, Mail Stop D466, Los Alamos, NM.

[†]Staff Scientist, Applied Mathematics and Plasma Physics (T-5), Los Alamos National Laboratory, P.O. Box 1663, Los Alamos, NM.

[‡]Ph.D. Candidate, University at Buffalo, State University of New York, Buffalo, NY

[§]Deputy Group Leader, Space Science and Applications (ISR-1), Los Alamos National Laboratory, P.O. Box 1663, Mail Stop D466, Los Alamos, NM.

assumed that orbit estimates were available for each satellite at an arbitrary time interval, (3) the ballistic coefficients were modeled as constants and were assumed known to within 5% of the true value.

The goal of the present work is to show the applicability of this tomography-based method to a realistic ground-based sensor network, set of target satellites, and orbit estimation system. Specifically, we identify a set of actual satellites in orbit that would be suitable tracking candidates, i.e. passing through the defined density grid and unlikely to be actively conducting orbital maneuvers. We use the publicly available two-line element sets (TLEs) for these objects as initial conditions for an orbit propagator, and then simulate the orbits of these satellites over several days. Simulated tracking measurements (i.e. angle measurements from a ground-based optical sensor) are generated with added noise. These tracking measurements are then processed in a Constrained Admissible Region Multiple Hypothesis Filter (CAR-MHF) to generate estimates of the satellite position, velocity, and ballistic coefficient. The CAR-MHF has been demonstrated in the past on GEO satellites with solar radiation pressure effects,[3,4] and more recently for LEO satellites with drag effects.[5] The CAR-MHF algorithm provides a means for initial orbit determination, with quantifiable uncertainty, and requires no a priori state information on the orbits or ballistic coefficients. Its potential value to this work is the ability to process spatially and temporally distributed observations in an automated fashion, thus opening up a wider range of LEO objects (e.g. space debris) that could be used as input to the orbit tomography process.

One advantage of the tomography-based approach is that a small number of ground sites could be used to estimate corrections to the global density model, in contrast with existing methods that use a larger number of sensors. However, the success of the method is dependent on having a suitable set of tracking targets. This research demonstrates the feasibility of providing an end-to-end solution for converting satellite tracking measurements into density corrections based on data from a limited sensor network such as assumed in our simulation. These improved density measurements can then be incorporated into physics-based (i.e. predictive) density models for improved orbit propagation accuracy. This research is tied to a multi-year, internally funded project at Los Alamos National Lab called Integrated Modeling of Perturbations in Atmospheres for Conjunction Tracking (IMPACT)*, which targets several areas of thermospheric density modeling and prediction,[6] satellite drag modeling,[7,8] and conjunction analysis.

GROUND-BASED TRACKING

This study assumes a single ground site located near Los Alamos, New Mexico. Such a system currently exists for space situational awareness research, which uses a 14-inch diameter Celestron C-14 Schmidt-Cassegrain telescope on a Paramount German equatorial mount, with a field-of-view of 0.9 deg. The site, named Fenton Hill, is located in the Jemez Mountains near Fenton Lake, with coordinates of 35.881 deg latitude, -106.674 deg longitude, and 2.66 km altitude.

TARGET SELECTION

This section describes the process of selecting targets for this simulation. The simulation uses an observation time span from t_0 =2011-6-21 00:00:00 UTC and lasting for six days until 2011-6-27 00:00:00 UTC. The publicly available space catalog† is searched for resident space objects (RSOs)

*http://impact.lanl.gov

†http://www.space-track.org

that may be potential targets to apply to the tomography method during this time period. Objects that satisfy the following criteria are first selected:

- Indication of non-maneuvering or inactive object:
  - Names with "DEB" (debris), "R/B" (rocket body), etc. which are almost certainly non-maneuvering.
  - Satellites launched prior to 1990, which are assumed for this simulation to be inactive.
  - Satellites that decayed between the t_0 epoch and the current time (e.g. uncontrolled cubesats), the assumption being that if they decayed fairly recently, then they may have been inactive or near the ends of their useful missions.
- Apogee below 700 km altitude
- Radar cross-section (RCS) above 0.05 m^2

Inactive or non-maneuvering objects are good candidate targets because the decay due to atmospheric drag is directly observable. Objects that perform orbital maneuvers can still in principle be used, but the process of detecting and correcting for the orbit raising greatly complicates the process. The RCS limit is chosen based on the capabilities of the assumed optical telescope and camera, i.e. the current system has successfully observed debris fragments with cataloged RCS values down to approximately 0.05 m^2. Thus, we assume that any object with a published RCS value greater than 0.05 m^2 will be detectable with our observation system.

Figure 1 shows the altitudes of perigee and apogee for each of the above selected candidate RSOs (numbering 208 objects in total). These candidate objects are further down-selected to a subset of 47 objects, described in Table 1, which have suitable visibilities during the simulation period in question. Here, we define suitabile visibiltiles to mean having at least one pass per day at Fenton Hill, when the satellite is illuminated by the Sun while the ground site is in darkness, and with minimum elevation of 10 deg. The last set of points indicated in Fig. 1 represent those RSOs that were successfully estimated in the CAR-MHF (discussed below).

ORBIT SIMULATION

The TLEs for each of the RSOs in Table 1 are converted to cartestian position and velocity in the J2000 frame at the t_0 epoch. For the purposes of this simulation, a "truth" ballistic coefficient $\beta = C_D A/m$ is defined for each object by sampling from a uniform distribution between 0.001 and 0.01 m^2/kg. The truth orbits are propagated using a 6×6 EGM96 gravity field, lunisolar third-body gravity, and atmospheric drag using the Global Ionosphere-Thermosphere Model (GITM)[9] for the neutral density and a corotating wind model to compute velocity relative to the freestream. Solar radiation pressure is not applied for simplicity, but since the target orbits are below 700 km altitude, this omission will not greatly affect the simulation's realism. The measured topocentric right-ascension and declination angles as seen from Fenton Hill are synthesized from these truth orbits, at 1 Hz measurement frequency, with added Gaussian noise of 1.0 arcsec (1-σ) in each angle component.

Table 1: Candidate RSOs having suitable visibilities at Fenton Hill during the observation time span, where the apogee and perigee heights represent the approximate values at t_0 =2011-6-21. RCS = radar cross section.

NORAD ID	Name	RCS (m^2)	Launch	Decay	h_p (km)	h_a (km)
4863	THORAD AGENA D DEB	0.058	1970-04-08	2011-12-01	554	555
5133	THORAD AGENA D DEB	0.056	1970-04-08	2012-11-15	582	635
7338	SL-8 R/B	4.702	1974-06-18	2012-06-22	313	540
12054	COSMOS 1220	10.59	1980-11-04		444	522
12770	COSMOS 1275 DEB	0.070	1981-06-04	2011-11-03	450	485
13153	COSMOS 1356	9.45	1982-05-05		508	524
14207	COSMOS 1484	5.97	1983-07-24	2013-01-28	390	429
16111	SL-3 R/B	5.93	1985-10-03		492	517
19241	COSMOS 1666 DEB	0.11	1985-07-08	2012-07-07	405	416
23906	HILAT DEB	0.19	1983-06-27	2011-12-02	491	499
24925	DUMMY MASS 1	1.45	1997-09-01		611	630
24926	DUMMY MASS 2	1.45	1997-09-01		592	625
25795	COSMOS 1220 DEB	0.051	1980-11-04		494	661
26034	CELESTIS 03/TAURUS R/B	1.23	1999-12-21		601	643
26130	CZ-4 DEB	0.065	1999-10-14	2011-08-06	395	450
26139	CZ-4 DEB	0.19	1999-10-14	2012-08-20	491	523
26172	CZ-4 DEB	0.098	1999-10-14		502	581
26195	CZ-4 DEB	0.057	1999-10-14	2013-02-15	504	531
26213	CZ-4 DEB	0.13	1999-10-14	2012-09-26	458	520
26230	CZ-4 DEB	0.26	1999-10-14		525	561
26415	MINOTAUR R/B	1.61	2000-07-19		439	473
26551	DNEPR 1 DEB	2.46	2000-06-10	2012-06-10	467	500
27068	PSLV DEB	0.097	2001-10-22		439	536
27134	PSLV DEB	0.14	2001-10-22	2012-06-04	451	515
27644	DELTA 2 DEB (DPAF)	6.39	2003-01-13		506	540
28643	PEGASUS R/B	1.12	2005-04-15	2012-01-31	357	432
28738	CZ-2D R/B	12.7	2005-07-05		542	561
28812	SL-24 DEB	1.25	2005-08-23		585	623
28813	SL-24 DEB	9.70	2005-08-23		562	603
29659	SL-8 R/B	4.58	2006-12-19		440	492
29823	FENGYUN 1C DEB	0.058	1999-05-10	2011-10-03	385	539
30187	FENGYUN 1C DEB	0.058	1999-05-10	2011-09-16	416	540
30778	ATLAS 5 CENTAUR R/B	8.94	2007-03-09		495	533
31798	SL-8 R/B	4.11	2007-07-02		452	490
32790	CANX-2	0.069	2008-04-28		591	639
33085	COSMOS 2421 DEB	0.053	2006-06-25	2012-01-24	374	573
33102	COSMOS 2421 DEB	0.051	2006-06-25	2012-01-28	376	564
33245	SL-8 R/B	4.61	2008-07-22		451	490
33807	COSMOS 2251 DEB	0.050	1993-06-16	2011-11-14	343	555
33925	COSMOS 2251 DEB	0.056	1993-06-16	2011-11-16	584	665
34808	ANUSAT	0.46	2009-04-18	2012-04-18	394	503
34844	CZ-2C DEB	0.081	2009-04-22	2012-08-26	446	627
35001	TACSAT 3	2.51	2009-05-19	2012-04-30	411	430
35002	PHARMASAT	0.022	2009-05-19	2012-08-14	407	436
35006	MINOTAUR R/B	1.35	2009-05-19	2012-11-05	411	436
36801	PSLV DEB	2.52	2010-07-12		630	634

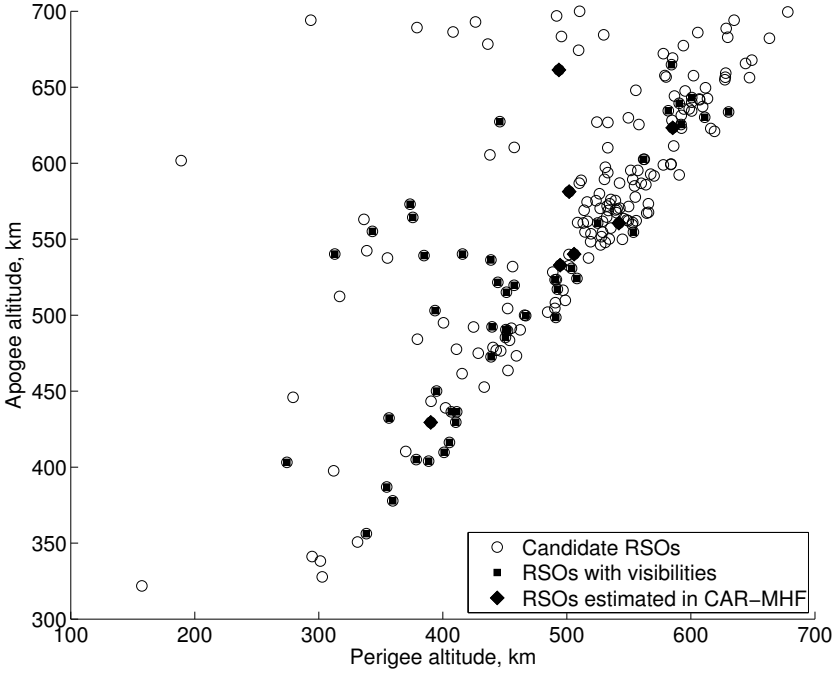

Figure 1: Apogee and perigee altitudes of the candidate RSOs (white circles), those RSOs having the required visibilities (black squares), and those successfully estimated in the CAR-MHF (black diamonds).

CAR-MHF ORBIT ESTIMATION

The propagator in the CAR-MHF also uses the same force model described above to propagate the truth orbits, with the exception of the density model: here, we use a simple static exponential model, using tabulated values of the density scale height and reference density taken from pp. 537 of Ref. 10, which are based on the CIRA-72 model.

The eventual goal for the envisioned system being simulated in the present study is to use the CAR-MHF to estimate the orbit states and drag ballistic coefficient, and then feed these into the tomography method to estimate the atmospheric density corrections. For the current simulations, the CAR-MHF was not successfully applied to all of the 47 objects in Table 1. Rather, only seven objects successfully converged to orbit estimates that were within the predicted uncertainties. The errors on the final state estimates after 5 days of tracking for these seven objects were approximately 10 m (1-σ) in position and 1 cm/s (1-σ) in velocity. The likely reason for the poor performance of the CAR-MHF in this case is the large discrepancy between the truth density model (GITM) and the density model used in the CAR-MHF propagator, which is discussed in more detail below.

TOMOGRAPHY SIMULATION

The premise behind the tomography simulation in this study is to take the state estimates at t_1 and t_2 for each RSO, compute the measured change in orbital specific mechanical energy over that time span, and solve for the spatially resolved, yet time-averaged, density scale factor $s = \rho_{\mathrm{true}}/\rho_{\mathrm{mod}}$,

where ρ_{true} is the true density, and ρ_{mod} is the modeled density. Here, we use $t_1 = t_0 + 3.5$ days and $t_2 = t_0 + 5.5$ days; hence, the measured decay in orbital specific mechanical energy takes place over roughly 48 hrs.

Because not enough RSOs were successfully processed in the CAR-MHF, we simulated the state estimates of the remaining objects from the set of 47 RSOs with suitable visibilities. This was done by taking the truth state at t_1 and t_2 and adding simulated state estimation error based on the approximate covariance from the 7 RSOs that were estimated in the CAR-MHF. Gaussian error with 1-σ variance of 10 m in position and 1 cm/s in velocity was added to each of the state elements at t_1 and t_2. In addition to the orbit estimation error at t_1 and t_2, the other main source of error in the tomography process is the assumed ballistic coefficient that is used to propagate the reference orbit from t_1 to t_2.

The follow subsections describe two sets of tomography results, which use different modeled densities ρ_{mod}: (1) using the same static exponential model as was used in the CAR-MHF propagator, and (2) using the NRLMSISE-00 density model. All of the tomography results described here use a global grid spanning from 350 to 600 km altitude, with 20 deg spacing in latitude and longitude and 125 km spacing in altitude. The resulting grid has 324 cells in total, with two altitude slices centered on 412.5 and 537.5 km.

Using static exponential model for ρ_{mod}

Figures 2a and 2b show the true time-averaged s over the 48 hr tomography time span $t_2 - t_1$ at the two altitude slices. Here, the true ballistic coefficient β is used without additional error to propagate the reference trajectory. The magnitude of s shows large variations between approximately 1 and 4 in these plots, because the simple static exponential model is an averaged model (both temporally and spatially), e.g. it does not capture the diurnal variations, whereas GITM is a physics-based model that captures these dynamics.

Figures 3a and 3b show the resulting estimated s fields from the tomography. The estimated slice at 412.5 km shows some qualitative agreement to the truth; the increase and decrease around 150 and 0 deg longitude, respectively, are somewhat apparent, but the magnitude of these values are off by over 50%. Likewise, the estimated slice at 537.5 km shows virtually no agreement to the truth. Thus, even assuming perfect knowledge of β, the tomography result using the static exponential model would be inadequate for our needs.

Using NRLMSISE-00 for ρ_{mod}

Figures 4a and 4b show the corresponding true time-averaged s slices when using NRLMSISE-00 as ρ_{mod}. Here, we add error of 10% (1-σ) to the true β when propagating the reference trajectory, to simulate imperfect knowledge of each satellite's ballistic coefficient. In contrast with the results of the previous subsection, here we see that GITM and NRLMSISE-00 are similar because the true s is closer to unity. Figure 5a shows that the tomography in this case is able to estimate some of the spatial features seen in Fig. 4a , such as the peak around $s = 0.7$ at 150 deg longitude, and the valley around $s = 0.5$ at 0 deg longitude. In general, when comparing Figs. 4a and 5a, it is apparent that the estimated values are within a few percent of the true values.

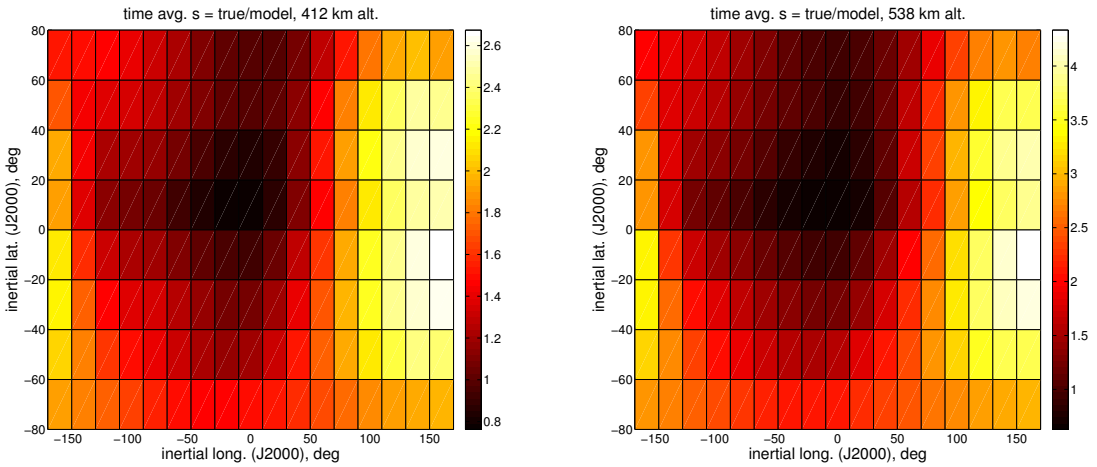

(a) Altitude slice at 412.5 km.

(b) Altitude slice at 537.5 km.

Figure 2: True time-averaged s, where $\rho_{\text{mod}} =$ simple exponential model.

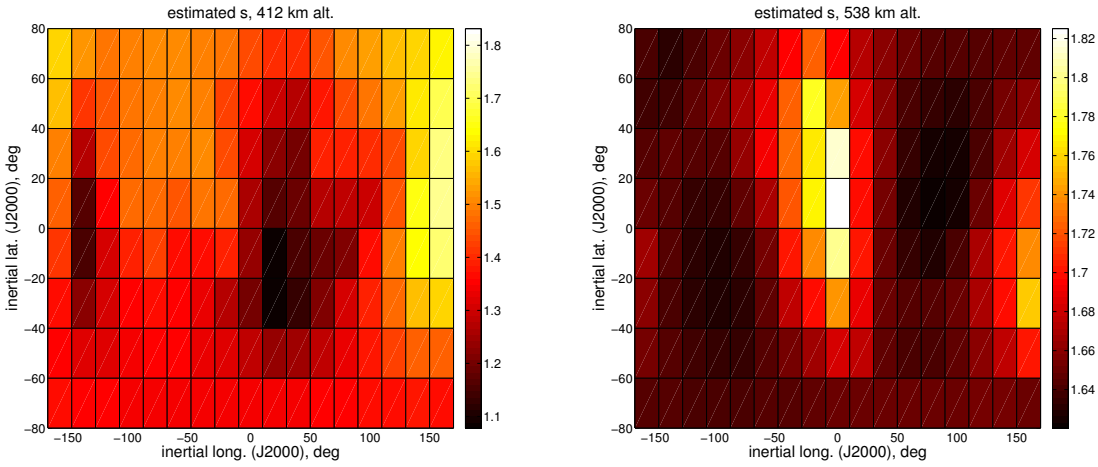

(a) Altitude slice at 412.5 km.

(b) Altitude slice at 537.5 km.

Figure 3: Estimated time-averaged s, where $\rho_{\text{mod}} =$ simple exponential model.

BALLISTIC COEFFICIENT ESTIMATION

The CAR-MHF results for estimating the position and velocity were discussed above. Here, we discuss the estimated ballistic coefficient; it must be noted that the MHF's estimate of β is biased by the density model used in the CAR-MHF's propagator. Figure 6 shows the ratio of the estimated β to the true β for all seven objects in the bottom plot, and for just one object (14207) in the top plot for clarity as an example. If the density model in the CAR-MHF's propagator matched the true density model (i.e. that used to propagate the truth orbits), then one would expect the ratio plotted

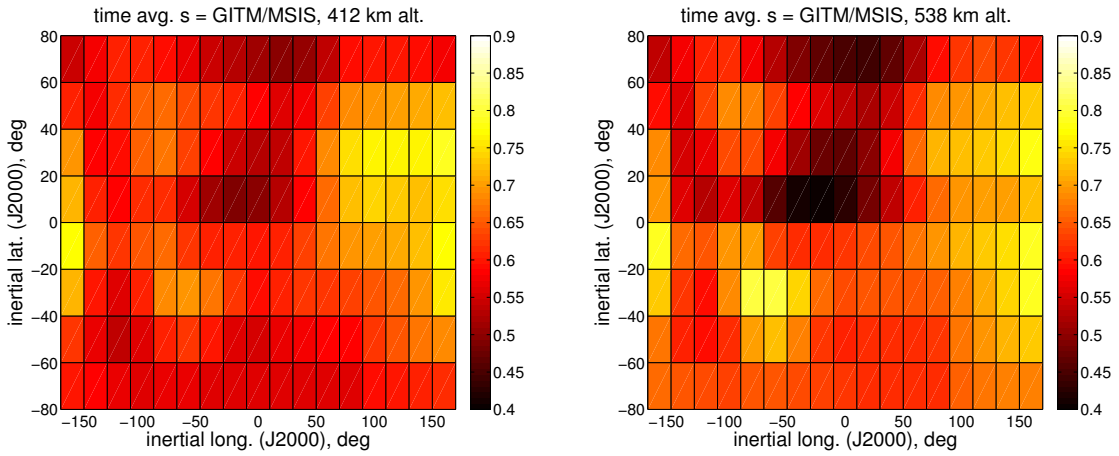

(a) Altitude slice at 412.5 km.

(b) Altitude slice at 537.5 km.

Figure 4: True time-averaged s, where $\rho_{\text{mod}} =$ NRLMSISE-00.

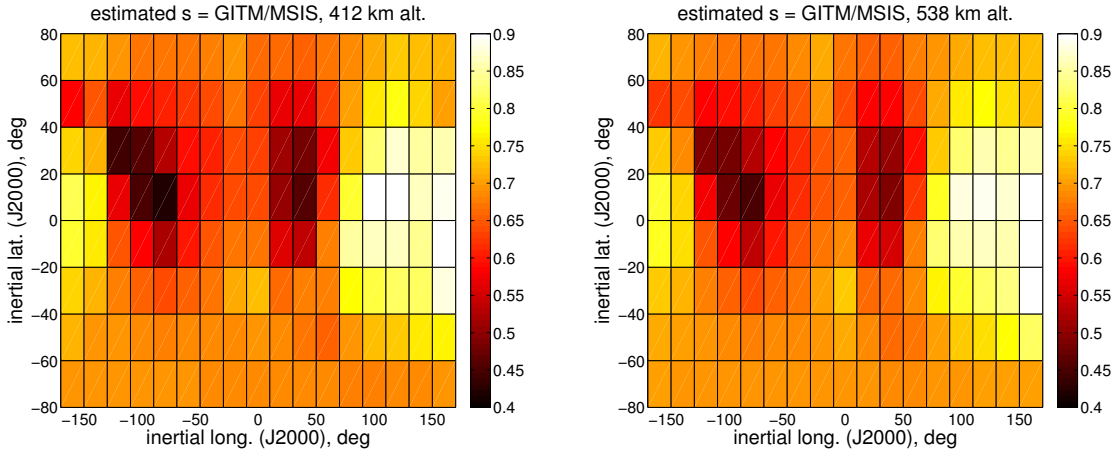

(a) Altitude slice at 412.5 km.

(b) Altitude slice at 537.5 km.

Figure 5: Estimated time-averaged s, where $\rho_{\text{mod}} =$ NRLMSISE-00.

in Fig.6 to approach unity if the CAR-MHF were accurately estimating β. Recalling Fig.2a, and noting from Table 1 that object #14207 is orbiting at around 400 km, then it is expected that the ratio of estimated to true β shown in the top plot of Fig. 6 is around 2. Likewise, the bottom plot in Fig. 6 shows that all objects converge to ratios of estimated-to-true β of around 2 to 4, which reflects the true s values shown in Figs.2a and 2b.

Thus, in order to pass an accurate estimate of β to the tomography, these biases need to be reduced. One way to do this is to compare the estimated β for a given object with a predicted value (e.g. for simple shapes like cubesats or rocket bodies that can be modeled with reasonable accuracy). Once the approximate global s factor is known for this "calibration" satellite, i.e. given

the estimated β from the CAR-MHF and the "true" value of β, then we can use this to approximately correct the estimated β for all of the other satellites. This process is similar in principle to that used by HASDM, where long-term estimates of β for some calibration targets are averaged and used as the "true" β values.[11] Further simulations of the tomography method described in this paper are needed to understand the required accuracy on the estimated β.

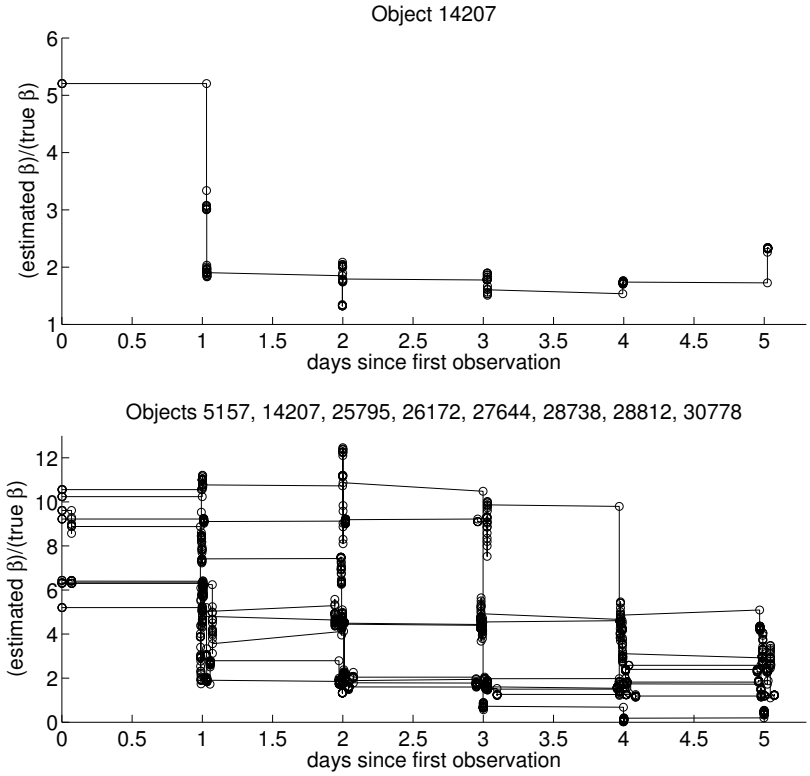

Figure 6: Ratio of estimated-to-true β using the CAR-MHF.

CONCLUSION

Of the 208 candidate tracking targets identified in this study, nearly 50 had suitable visibilities from the single ground site in New Mexico to allow sufficient measurements over six days. The truth orbits were simulated using the GITM atmospheric density model, and the CAR-MHF used a simple exponential density model in its propagator. Because of the large discrepancies between these two density models, the CAR-MHF was only successful in estimating the orbits of seven of the tracking targets. However, this result gives us a reasonable quantification of the expected orbit estimation accuracy for the assumed system, and we expect the CAR-MHF performance to improve when using a more accurate density model. The remaining objects are processed in the tomography method, assuming orbit estimation error of 10 m in position and 1 cm/s in velocity. Over a tomography time span of 48 hours, and assuming NRLMSISE-00 as the modeled density, the tomography is able to reconstruct the true time-averaged density to within several percent. These results suggest that the single ground site in New Mexico with realistic target satellites can feasibly reconstruct the spatially resolved global density field. However, further simulations are required to

verify the performance of the CAR-MHF for a larger set of targets and when the tomography has an imperfect knowledge of the ballistic coefficient.

ACKNOWLEDGMENTS

This work was conducted under the auspices of the U.S. Department of Energy, with support from the Los Alamos National Laboratory (LANL) Directed Research and Development program. We thank Tom Kelecy of The Boeing Company and Moriba Jah of Air Force Research Laboratory for providing support with the CAR-MHF. We also thank Humberto Godinez and Andrew Walker of LANL for generating the GITM and MSIS atmospheric density data used in this study.

NOTATION

A	drag cross-sectional area, km^2
C_D	drag coefficient, unitless
h_a	altitude of apogee, km
h_p	altitude of perigee, km
m	mass, kg
s	scale factor on modeled density, unitless
β	drag ballistic coefficient, m^2/kg
ρ_{mod}	modeled density, kg/km^3
ρ_{true}	true density, kg/km^3

REFERENCES

[1] M. Shoemaker, B. Wohlberg, and J. Koller, "Atmospheric Density Reconstruction Using Satellite Orbit Tomography," *23rd AAS/AIAA Spaceflight Mechanics Meeting, Feb. 2013, Kauai, HI*.

[2] M. Shoemaker, B. Wohlberg, and J. Koller, "Atmospheric Density Reconstruction Using Satellite Orbit Tomography," *Journal of Guidance, Control, and Dynamics*, 2013. under review.

[3] K. DeMars, M. Jah, and P. Schumacher Jr., "Initial Orbit Determination using Short-Arc and Angle Rate Data," *IEEE Transactions on Aerospace and Electronic Systems*, Vol. 48, July 2012, pp. 2628–2637.

[4] T. Kelecy, M. Jah, and K. DeMars, "Application of a Multiple Hypothesis Filter to near GEO high area-to-mass ratio space objects state estimation," *Acta Astronautica*, Vol. 81, No. 2, 2012, pp. 435–444.

[5] T. Kelecy, M. Shoemaker, and M. Jah, "Application of the Constrained Admissible Region Multiple Hypothesis Filter to initial Orbit Determination of a Break-Up," *6th European Conference on Space Debris, 22-25 April, Darmstadt, Germany*, 2013.

[6] H. C. Godinez, B. Nadiga, A. J. Ridley, J. Koller, E. Lawrence, and D. Higdon, "Atmospheric Density Specification with the Global Ionosphere-Thermosphere Model (GITM) using the Ensemble Kalman Filter," 2012. Poster at the American Geophysical Union Fall Meeting 2012, San Francisco CA, December 3-7.

[7] A. Walker, P. Mehta, and J. Koller, "A Quasi-Specular Drag Coefficient Model using the Cercignani-Lampis-Lord Gas-Surface Interaction Model," *Journal of Spacecraft and Rockets*, 2013. under review.

[8] A. Walker, J. Koller, and P. Mehta, "A Comparison of Different Implementations of Diffuse Reflection with Incomplete Accommodation for Satellite Drag Coefficient Modeling," *Journal of Spacecraft and Rockets*, 2013. under review.

[9] A. J. Ridley, Y. Deng, and G. Toth, "The global ionosphere-thermosphere model," *Journal of Atmospheric and Solar-Terrestrial Physics*, Vol. 68, May 2006, pp. 839–864, doi:10.1016/j.jastp.2006.01.008.

[10] D. A. Vallado, *Fundamentals of Astrodynamics and Applications*. Microcosm Press, El Segundo, California, and Kluwer Academic Publishers, Dordrecht, The Netherlands, second ed., 2004.

[11] B. R. Bowman, "True Satellite Ballistic Coefficient Determination for HASDM," *AIAA/AAS Astrodynamics Specialist Conference, Aug. 2002, Monterey, CA*, 2002. AIAA Paper 2002-4887, doi:10.2514/6.2002-4887.